Field Theoretic CAD of Open or Aperture Matched T-Junction Coupled Rectangular Waveguide Structures

Thomas Sieverding and Fritz Arndt, *Senior Member, IEEE*

Abstract—**The rigorous computer-aided design of rectangular waveguide structures is described which are coupled by open or rectangular iris loaded *E*- or *H*-plane T-junctions. The design theory is based on the full wave mode-matching method for the key-building block T-junction element associated with the generalized *S*-matrix technique for composite structures. The waveguide structures may be arbitrarily composed of the T-junction and already known key-building block elements (such as the double step and the septum discontinuity) combined with homogeneous waveguide sections between them. The *E*- or *H*-plane T-junction effect, large apertures, finite iris or septum thicknesses and higher order mode interactions at all step discontinuities are rigorously taken into account. Typical design examples, like rectangular iris coupled T-junctions, narrow-stopband waveguide filters, high return loss *E*-plane T-junction diplexers, an elliptic function *E*-plane integrated metal insert filter and a simple ortho-mode transducer demonstrate the efficiency of the method. The theory is verified by measurements.**

I. Introduction

THE OPEN or aperture-coupled T-junction is a fundamental circuit element [1]–[8] in rectangular waveguide structures which is applied extensively for many components, such as for the design of bandstop-filters [2], manifold multiplexers [4], or couplers [5]. Many refined theories are available [1], [2], [4]–[8] for deriving the corresponding equivalent circuit elements. However, the increasing demand for compact and low-cost components as well as the growing interest in the millimeter wave frequencies have prompted the need for more accurate methods which take adequately into account the junction effect, large apertures, their finite thickness, and the higher-order mode interactions of all discontinuities involved. Moreover, the availability of high-precision fabrication techniques requires design methods without the necessity for additional "trial-and-error" adjustment aids like tuning screws. Although an exact calculation for the rectangular waveguide T-junction equivalent circuit parameters is available for a long time [3], no rigorous analysis for the general rectangular aperture-coupled T-junction, as well as for the components utilizing this circuit element, has been derived so far.

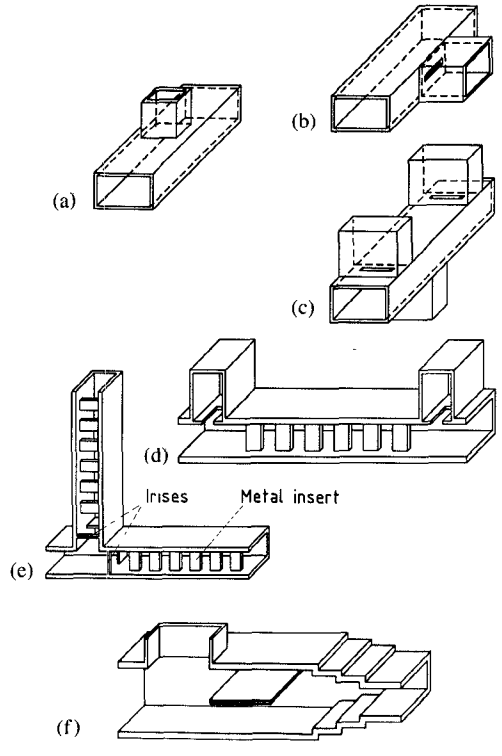

Fig. 1. A class of waveguide components where the structures or filter sections are combined by open or aperture-coupled T-junctions: (a) T-junction with sidearm of reduced cross-section dimension. (b) Aperture-coupled T-junction. (c) Bandstop resonator cavity filter. (d) *E*-plane integrated circuit filter with additional aperture-coupled bandstop cavities. (e) *E*-plane T-junction diplexer with iris matching elements. (f) Simple ortho-mode transducer.

This paper presents a rigorous computer-aided design method for the class of waveguide components shown in Fig. 1, where the waveguide structures or filter sections are combined by open (Fig. 1(a)) or aperture-coupled T-junctions (Fig. 1(b)): The bandstop resonator cavity filter (Fig. 1(c)), the *E*-plane integrated circuit filter with additional aperture-coupled bandstop cavities (Fig. 1(d)), the *E*-plane T-junction diplexer with iris matching elements (Fig. 1(e)), and the simple ortho-mode transducer (Fig. 1(f)).

The design method proposed is based on the full wave

Manuscript received May 23, 1991; revised October 1, 1991.

The authors are with the Microwave Department, University of Bremen, Kufsteiner Str., NW1, D-2800 Bremen, Germany.

IEEE Log Number 9104785.

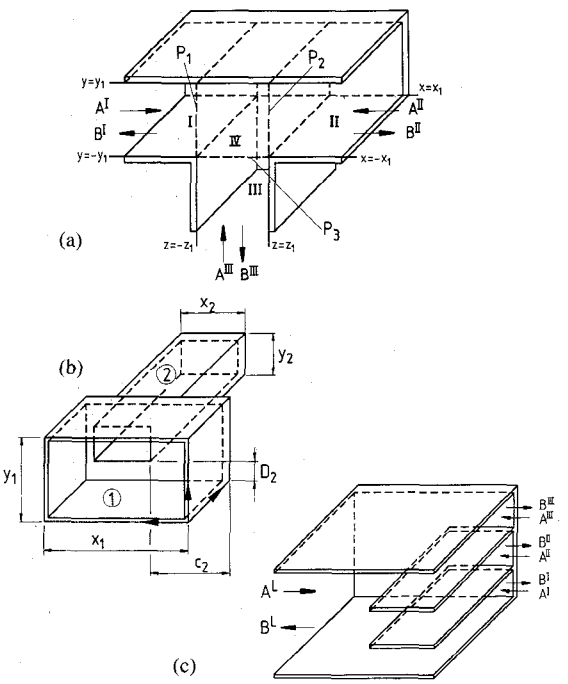

Fig. 2. General six-field component key-building block discontinuities. (a) T-junction (both *E*- and *H*-plane). (b) Rectangular waveguide double-step. (c) Rectangular waveguide *n*-furcation (both *E*- and *H*-plane).

mode-matching method for the T-junction key-building block element (Fig. 2(a)) associated with the generalized *S*-matrix technique [9]–[12] for composite structures. The combination with already known key-building block modal *S*-matrices, i.e. the double-step discontinuity (Fig. 2(b)) [9] and the septated waveguide section (Fig. 2(c)) [10], achieves the rigorous description of the composed waveguide circuits in Fig. 1.

The method includes the higher-order mode coupling effects, the finite thickness of all obstacles, and allows the passband and stopband characteristics of the filters or diplexers under investigation to be considered in the design. For comparison, analysis results are presented for the open *E*-plane T-junction with a sidearm of reduced cross-section according to Sharp [3], and for a slot-coupled *H*-plane T-junction given by Das *et al.* [8]. In contrast to [8], however, large slot heights may be rigorously included in the calculations.

For computer optimization of waveguide components, the evolution strategy method [10] is applied. Computer-optimized design examples are presented which demonstrate the efficiency of the described method: 1) a three-resonator bandstop filter in the waveguide *X*-band (8–12 GHz) with high peak stopband attenuation, 2) an *E*-plane metal insert filter with aperture-coupled stopband resonator sections which achieves an elliptic function behavior together with high return loss and—in contrast to metal insert coupled resonators [11]—high attenuation values over a broad frequency band, 3) an inductively matched *E*-band (60–90 GHz) *E*-plane T-junction metal insert diplexer with high return loss and stopband attenuation, and 4) a simple ortho-mode transducer for the separation of the TE_{10} and TE_{01} mode. The theory is verified by measurements at the individual T-junction as well as at composite structures.

II. Theory

For the rigorous computer-aided design of the filter structures to be investigated (Fig. 1), the full wave mode-matching method is applied for a few simple key-building block elements associated with the generalized *S*-matrix technique for composite structures [9]–[12]. Three key-building block elements (Fig. 2) are required to include all general cases under consideration (Fig. 1): The general T-junction (Fig. 2(a)), the rectangular double-step waveguide discontinuity [9] (Fig. 2(b)), and the general rectangular waveguide *n*-furcation [10] (Fig. 2(c)). The full-wave (six-field component) mode-matching method includes the asymmetric case for the double-step discontinuity as well as both the *E*-plane and the *H*-plane cases for the T-junction and *n*-furcation, Figs. 2. For the corresponding inverse discontinuities, merely the corresponding modal *S*-matrix of the original structure needs to be transposed [9]–[12].

As the modal *S*-matrices of the discontinuities in Fig. 2(b) and 2(c) have already been derived in [9] and [10], merely the T-junction key-building block element (Fig. 2(a)) needs further consideration. The full wave modal *S*-matrix of the T-junction is derived by applying the mode-matching procedure for suitably chosen subregions (Fig. 2(a)), like in the case of the *E*-plane T-junction [12], but now with the full set of TE_{mn} and TM_{mn} modes.

For the waveguide subregion ν under consideration, the fields [13]

$$\vec{E}^{\nu} = \frac{1}{j\omega\epsilon} \nabla \times \nabla \times \vec{A}_e^{\nu} + \nabla \times \vec{A}_h^{\nu}$$

$$\vec{H}^{\nu} = -\frac{1}{j\omega\mu} \nabla \times \nabla \times \vec{A}_h^{\nu} + \nabla \times \vec{A}_e^{\nu} \qquad (1)$$

are derived from the z components of the electric and magnetic vector potentials $\vec{A}_e$, $\vec{A}_h$, respectively,

$$\vec{A}_{hz} = \sum_{i=0}^{N_h} Q_{hi} T_{hi} [A_{hi} e^{-\gamma_{hi} z} + B_{hi} e^{+\gamma_{hi} z}] \qquad (2a)$$

$$\vec{A}_{ez} = \sum_{i=1}^{N_e} Q_{ei} T_{ei} [A_{ei} e^{-\gamma_{ei} z} - B_{ei} e^{+\gamma_{ei} z}] \qquad (2b)$$

where A_i, B_i are the still unknown eigenmode amplitude coefficients of the forward $(-)$ and backward $(+)$ waves in z direction, $\gamma_{h,e}$ are the propagation factors of the N_h and N_e considered TE_{pq} and TM_{pq} modes, respectively, where i stands for p, q; Q is a normalization factor, so that the power carried by each mode is 1 W for propagating modes, jW for evanescent TE modes, $-jW$ for evanescent TM modes [9]–[12], and T are the cross-section eigenfunctions

$$T_{hi} = D_p D_q \sqrt{Z_h} \cos\left(\frac{p\pi}{a} x\right) \cos\left(\frac{q\pi}{b} y\right) \qquad (3a)$$

$$T_{et} = \sqrt{Y_e} \sin\left(\frac{p\pi}{a} x\right) \sin\left(\frac{q\pi}{b} y\right), \tag{3b}$$

with

$$D_{p,q} = \frac{1}{\sqrt{1 + \delta_{0p,q}}},$$

δ is the Kronecker delta, and the wave impedances Z_h or admittances Y_e, respectively.

The field in the cavity subregion IV (Fig. 2(a)) is superimposed by three suitably chosen standing wave solutions [12]

$$A^{IV}_{h,e} = A^{IV(1)}_{h,e} + A^{IV(2)}_{h,e} + A^{IV(3)}_{h,e}, \tag{4}$$

where solution (1) is obtained if the boundary planes P_2 and P_3 (Fig. 2(a)) are short-circuited and P_1 is open; solutions (2) and (3) are found analogously.

By matching the tangential field components given by (1)–(4) at the common interfaces across the discontinuities $z = -z_1$, $y \in (-y_1, y_1)$; $z = z_1$, $y \in (-y_1, y_1)$; and $y = -y_1$, $z \in (-z_1, z_1)$, respectively and utilizing the orthogonal property of the modes [13], the still unknown amplitude coefficients can be related to each other in the form of the desired modal scattering matrix of the T-junction:

$$\begin{pmatrix} \underline{B}^{I} \\ \underline{B}^{II} \\ \underline{B}^{III} \end{pmatrix} = \begin{pmatrix} \underline{S}_{11} & \underline{S}_{21} & \underline{S}_{31} \\ \underline{S}_{12} & \underline{S}_{22} & \underline{S}_{32} \\ \underline{S}_{13} & \underline{S}_{23} & \underline{S}_{33} \end{pmatrix} \begin{pmatrix} \underline{A}^{I} \\ \underline{A}^{II} \\ \underline{A}^{III} \end{pmatrix} \tag{5}$$

where the matrix elements are elucidated in the Appendix. For deriving the submatrices in the modal S-matrix (5) a modified algorithm is used which requires only the inversion of the quadratic submatrix $\underline{Y}$

$$\underline{Y} = (a_{31} M_1 - a_{32} M_4 + a_{33})^{-1} \tag{6}$$

with a third of the size of the original matrix of the coupling integrals; the elements in (6) are also given in the Appendix.

For composite structures the generalized S-matrix technique [9]–[12] is used, i.e., the direct combination of the corresponding modal S-matrices of all key-building block discontinuities and of the intermediate homogeneous waveguide sections between them. The corresponding equations for the overall modal S-matrix (S^C) of a) two cascaded two-ports, b) a cascaded two- and a three-port, as well as c) two cascaded three-ports (where each port may carry N_e and N_h modes) are for completeness given in the Appendix. Note that only one matrix inversion of reduced order is required.

A computer program was written using the preceding relations and utilizing the evolution strategy method [10]–[12] for optimizing the geometrical parameters. For the field theory CAD of rectangular iris coupled structures, sufficient asymptotic behavior has been obtained by consideration of TE_{mn}- and TM_{mn}-modes up to $m = 5$, $n = 4$ in the waveguide sections with longer homogeneous dimensions (e.g., in the resonator sections of the filters), and $m = 15$, $n = 4$ in the more critical iris sections. For discontinuities including merely TE_{m0}-modes, i.e., metal insert filters, 15 modes have been considered during the optimization; the final results have been verified by the inclusion of 45 TE_{m0} modes. For structures with T-junctions, e.g. the diplexer of Fig. 1(e) TM_{m0}-modes up to the order $m = 19$, as well as TE_{mn}- and TM_{mn}-modes up to $m = 1$ and $n = 5$ have been considered for the optimization run. The typical computing time for optimizing a five-resonator metal insert filter (like those in Fig. 8) is about 6h cpu on an IBM RISC 6000; a complete diplexer (like those in Fig. 9(b)) is optimized within about 10h cpu.

III. Results

For a first verification of the theory, the scattering parameters of standard E- and H-plane T-junctions in the waveguide Ku-band (12–18 GHz, WR62 waveguide housing: 15.799 mm × 7.899 mm) are presented in Fig. 3(a) and (b). Good agreement may be stated between our theory (solid lines), measurements (Δ Δ Δ) and the calculations (□ □ □) using the TE^x_{1n}-mode approach for the E-plane case [12], or the TE_{m0}-mode approach in the H-plane case [14], respectively.

For the example of a WR-137 (34.85 mm × 15.799 mm) rectangular waveguide T-junction, with a reduced width (WR-90: 22.86 mm × 10.16 mm) side waveguide (port 3), Fig. 4 shows the comparison between the scattering parameters obtained by our modal-S-matrix method and by the exact equivalent circuit admittance matrix calculation by Sharp [3] which has been verified there also by measurements. Good agreement may be stated. The power coupling mechanism below and above the cutoff frequency of the side waveguide (at 6.56 GHz) may be clearly identified.

The H-plane slot-coupled T-junction [8] has attained considerable interest, e.g., for the applications in slotted waveguide antennas [15], [16] or cascaded waveguide sections [17]. For comparison with the variational formulation for narrow slot heights presented in [8], Fig. 5a shows the scattering parameters calculated with our method (solid lines) for the X-band example (8–12 GHz, WR90 housing: 22.86 mm × 10.16 mm) given in [8]. Good agreement may be stated with the calculations of [8] (□ □ □) for narrow slot heights ($d/w = 0.55$), cf., Fig. 5(a). The slot height d, however, has a considerable influence on the coupling behavior, as is demonstrated at the example of the scattering parameter S_{31} for various heights d (Fig. 5(b)).

The E-plane slot-coupled T-junction shows a similar behavior. This is demonstrated in Fig. 6(a) at the example of the waveguide Ku-band (12–18 GHz, WR62 housing: 15.799 mm × 7.899 mm). Good agreement with the measured values (□ □ □) may be stated. If the T-junction is short-circuited (Fig. 6(b)), a bandstop behavior is obtained. Also good agreement with measurements (□ □ □) may be shown.

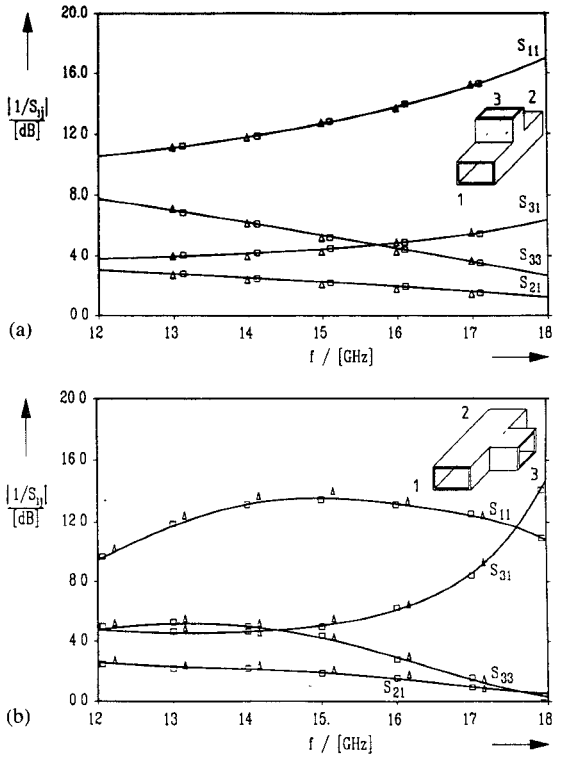

Fig. 3. Verification of the theory by standard (a) *E*- and (b) *H*-plane T-junctions. Waveguide *Ku*-band (12–18 GHz, WR62 waveguide housing: 15.799 mm × 7.899 mm). Our theory (solid lines), measurements (△ △ △) and the calculations (□ □ □) using the $TE_{1n}^{\downarrow}$-mode approach for the (a) *E*-plane case [12], or the TE_{m0}-mode approach in the (b) *H*-plane case [14], respectively.

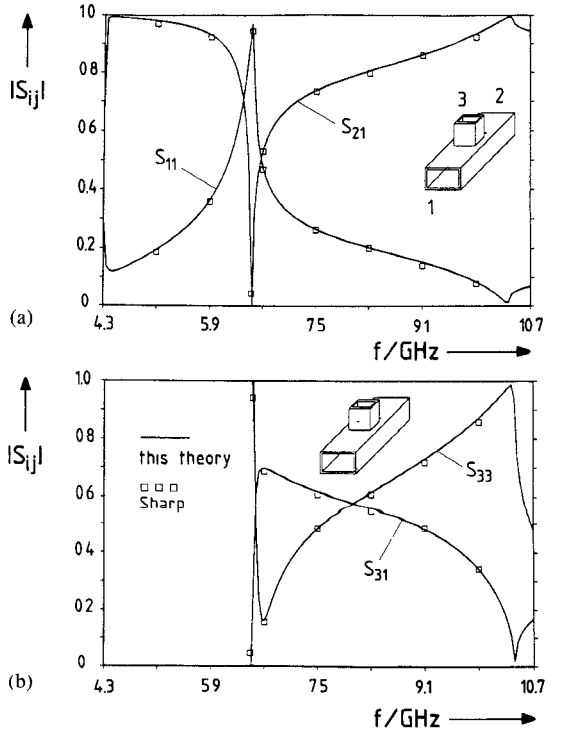

Fig. 4. WR-137 (34.85 mm × 15.799 mm) rectangular waveguide T-junction with a reduced width (WR-90: 22.86 mm × 10.16 mm) side waveguide (port 3). Comparison between the scattering parameters obtained by our modal-*S*-matrix method and by the exact equivalent circuit admittance matrix calculation by Sharp [3].

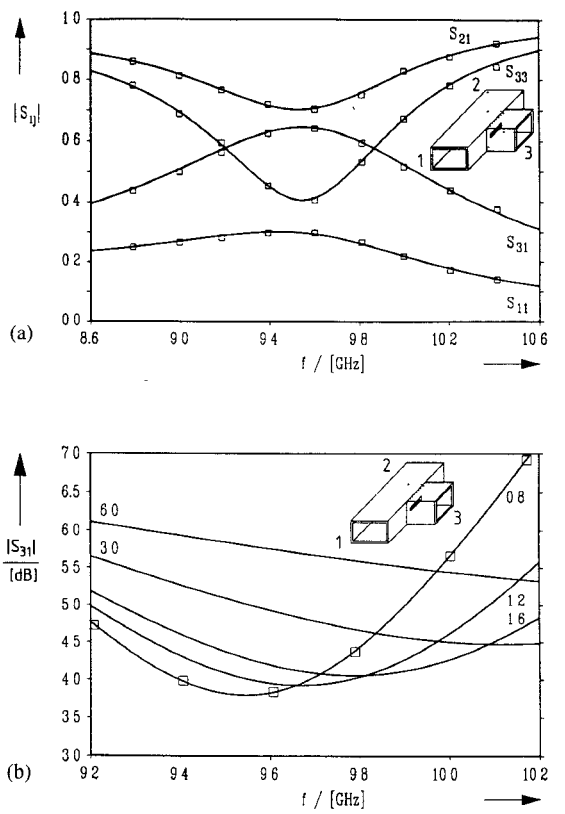

Fig. 5. *H*-plane slot-coupled T-junction. Scattering parameters calculated with our method (solid lines) and comparison with the variational formulation for narrow slot heights presented in [8] (□ □ □). (a) *X*-band example (8–12 GHz, WR90 housing: 22.86 mm × 10.16 mm) given in [8]. Iris thickness t = 1.27 mm, width w = 16 mm, height d = 0.8 mm. (b) Influence of the slot height d: example of a) but d = 0.8, 1.2, 1.6, 3, 6 mm.

A waveguide bandstop filter is conveniently realized [2] using aperture-coupled resonators connected in series and spaced an odd multiple of a quarter wavelength apart. Three-quarter intervals, instead of one-quarter spacing, is preferred [2] in order to reduce the otherwise strong interaction which would cause three peaks of high attenuation, instead of the desired single narrow-band peak. In order to verify the design theory presented in this paper also by a more complicated structure, Fig. 7 shows the calculated and measured insertion and return loss, respectively, of an *X*-band (8–12 GHz, WR-90 waveguide) bandstop filter example which has been constructed by using nearly the same dimensions as given in [2], but without the tuning screws. Good agreement between our calculations and measurements may be stated.

For many purposes, such as for channel filters, when frequency selectivity and high stopband attenuation over a broad frequency band are considered to be important filter properties, it may be highly desirable to improve the rejection quality of standard direct coupled cavity bandpass filters by utilizing additional stopband poles, as has been already realized by metal-insert coupled resonators [11], dual-mode filters [18], and asymmetric iris coupled filters [19]. Fig. 8 demonstrates a further design principle at the example of the computer-optimized results of a

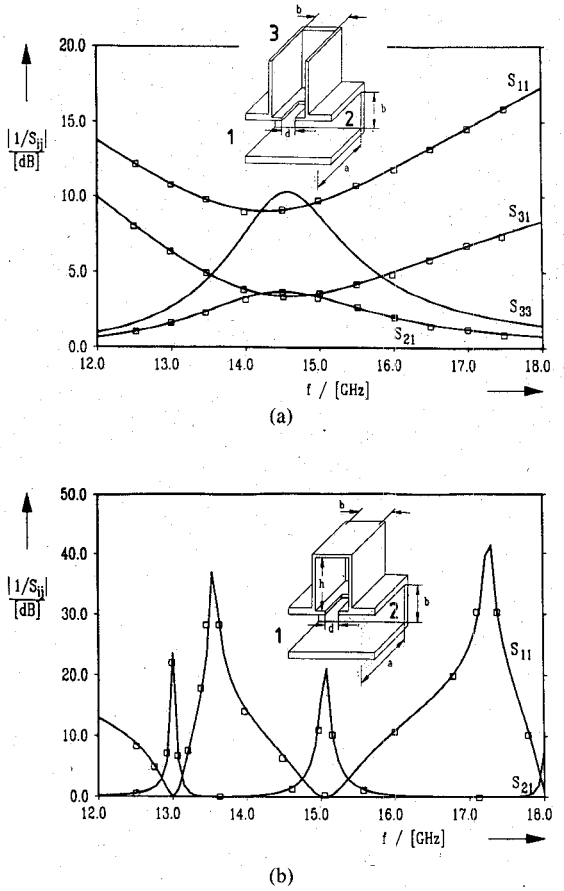

Fig. 6. The *E*-plane slot-coupled T-junction. Waveguide *Ku*-band (12–18 GHz, WR62 housing: 15.799 mm × 7.899 mm). Theory (——), comparisont with measurements (□ □ □). Slot width $w = 10.3$ mm, height $d = 3$ mm; thickness $t = 2.5$ mm. (a) Open T-junction. (b) Short-circuited T-junction, cavity height $h = 30$ mm.

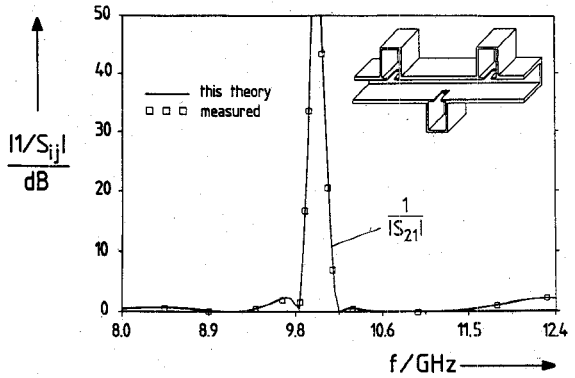

Fig. 7. Calculated (——) and measured (□ □ □) insertion loss of an *X*-band (WR-90 waveguide: 22.86 mm × 10.16 mm) bandstop filter example. Length between the resonators $l = 19.63$ mm, height of the outer resonators $h_1 = 16.54$ mm, of the inner resonator $h_2 = 16.94$ mm, iris thickness $t = 0.6$ mm, width $w_1 = 12.22$ mm, (inner iris $w_2 = 11.63$ mm), height of all irises $d = 3.05$ mm.

Ku-band (WR-62 waveguide: 15.799 mm × 7.899 mm) metal-insert filter with additional aperture-coupled bandstop cavities. The filter shows elliptic-function behavior with high skirt selectivity similar to the dual-mode approach of orthogonal mode filters [18], but avoids the disadvantage of the relatively small second stopband of the

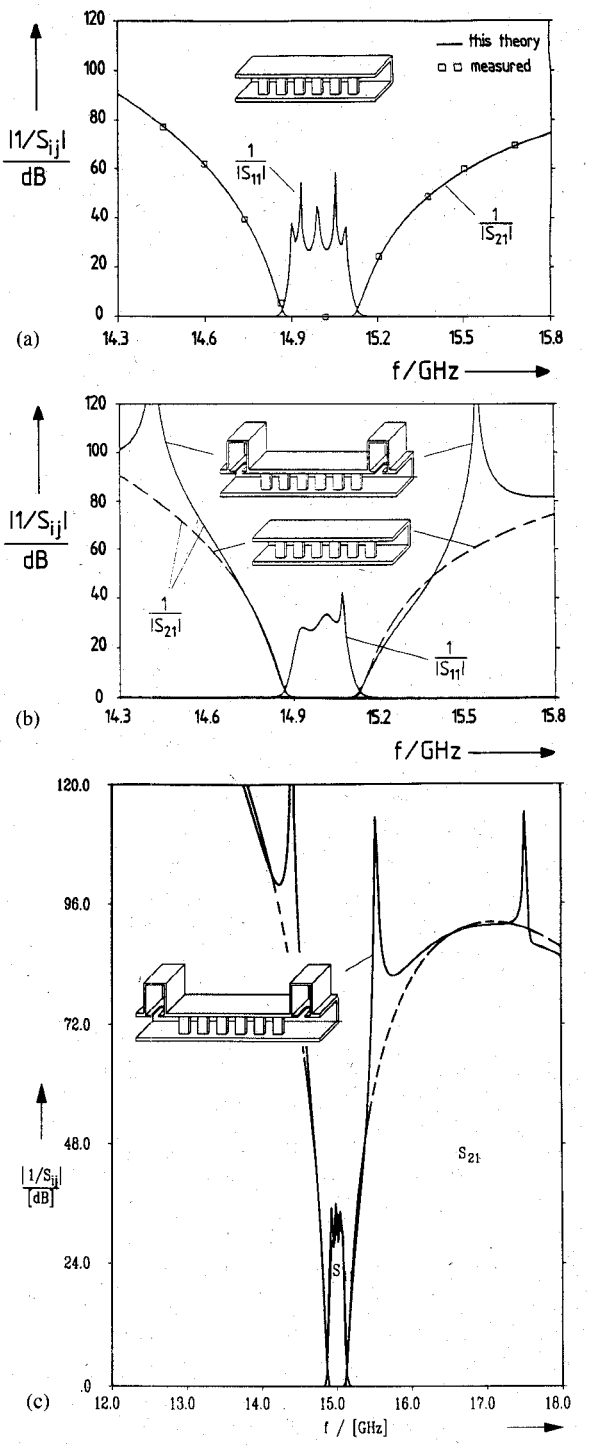

Fig. 8. Computer-optimized design results of a *Ku*-band (WR-62 waveguide: 15.799 mm × 7.899 mm) elliptic-function-type metal-insert filter with additional aperture-coupled bandstop cavities. Comparison with the single metal-insert filter. (a) Single metal-insert filter: Thickness of the inserts $t = 0.19$ mm; lengths (mid-plane symmetry) 3.111, 9.979, 11.446 mm; lengths of the resonator sections (mid-plane symmetry) 8.955, 8.968, 8.968 mm. (b) Additional iris-coupled stopband cavities: height of the cavities $h = 51.537$ mm, iris thickness $t = 2.106$ mm, height $d = 1$ mm, width $w = 9.807$ mm; distance between the cavities and the first and last metal insert, respectively, $l = 9.399$ mm. (c) Extended frequency scale of (b) in order to demonstrate the elliptic function behavior.

metal-insert coupled type [11]; this is due to the reduced interactions of the aperture-coupled cavities with the main filter section, in comparison with [11]. Moreover, very

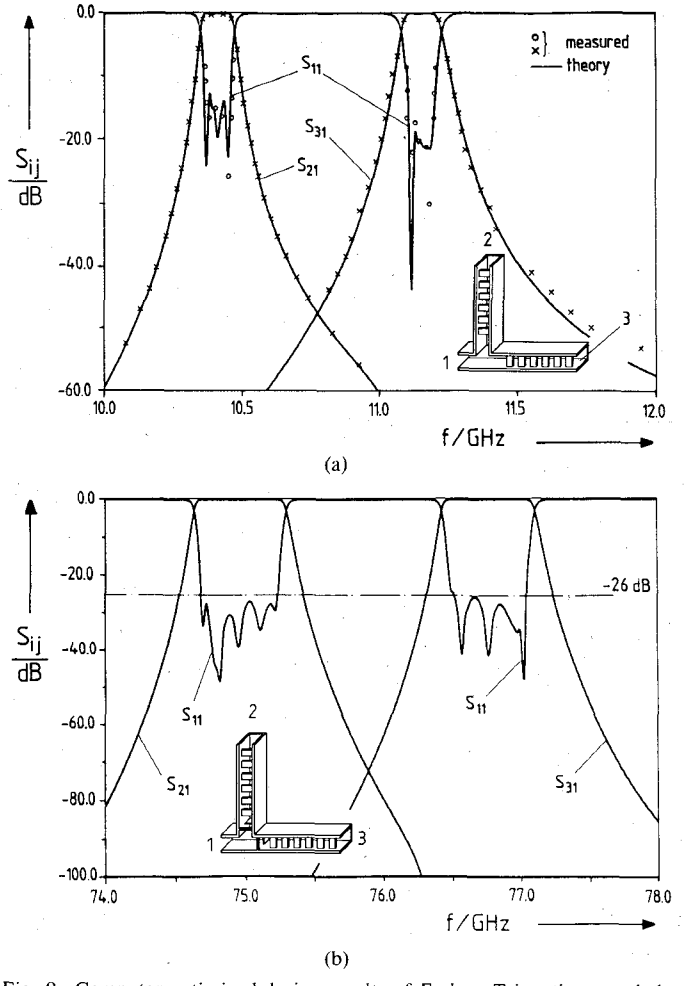

Fig. 9. Computer-optimized design results of E-plane T-junction coupled metal insert diplexers. (a) X-band (WR-90: 22.86 mm × 10.16 mm) diplexer with three-resonator filters. Comparison of calculated and measured insertion and return loss. Metal insert thickness $t = 0.19$ mm; filter in port 2 (midplane symmetry): metal insert lengths 3.112 mm, 10.077 mm, resonator lengths 17.437 mm, 17.596 mm; filter in port 3: 3.331 mm, 11.210 mm, resonator lengths 14.319 mm, 14.415 mm. (b) E-band (WR-12 waveguide: 3.099 mm × 1.549 mm) diplexer with additional matching irises of optimized dimensions and distance to the first filter section.

good return loss behavior is achieved by this design. This is demonstrated by comparison with the characteristic of the pure metal insert filter structure (Fig. 8(a)) which is nearly maintained in the overall design (Fig. 8(b)).

Fig. 9 show the computer-optimized design results of E-plane T-junction coupled metal insert filter diplexers. Very good agreement between the theoretically predicted values and the measurements may be stated (Fig. 9(a)) for the realized X-band type coupled with open T-junctions, where the matching is provided by optimizing the distance between the first metal-inserts and the T-junction (cf. Fig. 10). Additional matching irises, however, with optimized dimensions and distance to the first filter sections achieve diplexers with improved return loss behavior. This is demonstrated at the E-band (60–90 GHz, WR-12 waveguide: 3.099 mm × 1.549 mm) diplexer example presented in Fig. 9(b) which achieves overall 26 dB return

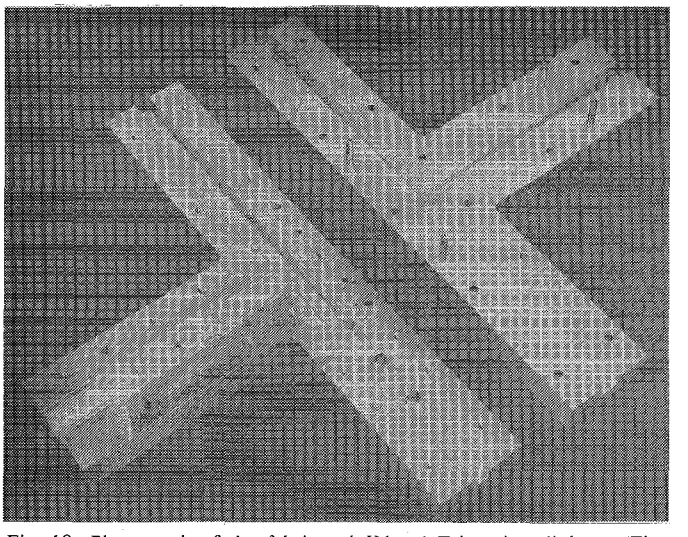

Fig. 10. Photograph of the fabricated X-band T-junction diplexer (Fig. 9(a)).

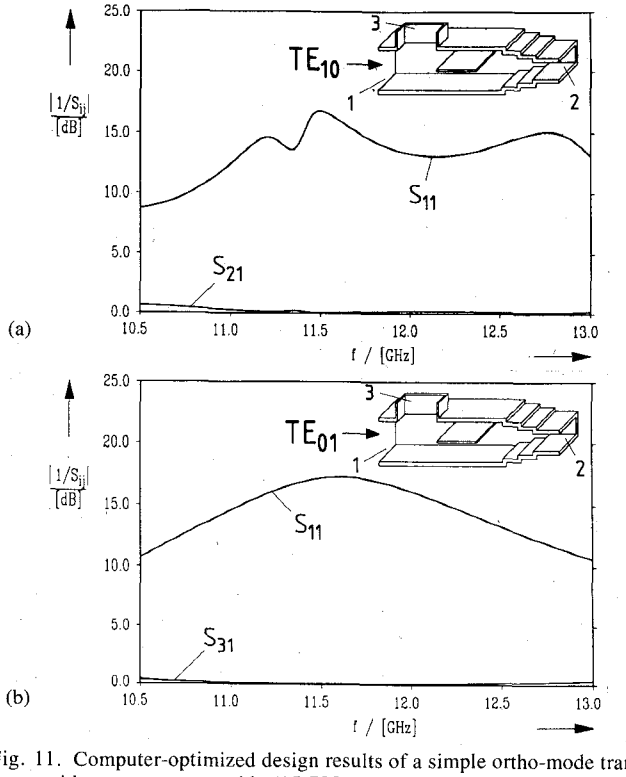

Fig. 11. Computer-optimized design results of a simple ortho-mode transducer with a square waveguide (15.798 mm × 15.798 mm) input port for both the orthogonal TE_{10} and TE_{01} modes. Port 2: WR-62 waveguide, 15.798 mm × 7.899 mm, port 3: 90° twisted WR-62 waveguide. Septum length $s = 10$ mm, thickness $t = 3$ mm; transformer section heights 10.765 mm, 15.228 mm, and lengths 5.544 mm, 8.636 mm; distance to septum 0 mm.

loss within both pass bands. The photograph of the fabricated X-band T-junction diplexer is shown in Fig. 10.

Fig. 11 presents the computer-optimized design results of a simple ortho-mode transducer with a square waveguide (15.798 mm × 15.798 mm) input port in order to supply both the orthogonal TE_{10} and TE_{01} modes simul-

taneously. The TE_{10} mode is transmitted to port 2 (WR-62 waveguide: 15.798 mm × 7.899 mm), whereas the TE_{01} mode is coupled to port 3 (90° twisted WR-62 waveguide). Although the return loss for this simple ortho-mode transducer without additional matching elements is not very high, good isolation between ports 2 and 3 is provided since the twisted rectangular waveguide output ports are below cutoff for the respective orthogonal mode.

IV. Conclusion

The modal *S*-matrix method described achieves the accurate design of a class of rectangular waveguide components where the waveguide sections, cavities or filter segments are combined by open or aperture-coupled T-junctions. Since the theory includes rigorously the *E*- or *H*-plane T-junction effect, large apertures, finite iris or septum thicknesses and higher order mode interactions at all step discontinuities, all relevant design parameters are taken into account in the optimization process. The results of computer-optimized design examples demonstrate the efficiency of the described design method: An *X*-band bandstop filter with high stopband attenuation, an elliptic-function-type *E*-plane metal insert filter with high return loss and high attenuation values over a broad frequency band, an *E*-band *E*-plane T-junction metal insert diplexer with high return loss, high skirt selectivity as well as broad second stopband, and a simple ortho-mode transducer. Measured results at single structures as well as at composed components verify the theory given by excellent agreement.

Appendix

Matrix Elements of the Modal S-Matrix in (5)

Matching the tangential electric field components at the common interfaces across the three discontinuities leads to the three unknown resonator amplitudes which may be expressed by the eigenmode amplitudes in the three ports:

$$R_h^{\mathrm{I}} = \frac{(A_p^{\mathrm{I}} + B_p^{\mathrm{I}})}{\sin(k_{z_p}^{\mathrm{I}} 2z_1)} \qquad R_e^{\mathrm{I}} = -j\frac{(A_p^{\mathrm{I}} + B_p^{\mathrm{I}})}{\sin(k_{z_p}^{\mathrm{I}} 2z_1)},$$

$$R_h^{\mathrm{II}} = \frac{(B_p^{\mathrm{II}} + A_p^{\mathrm{II}})}{\sin(k_{z_p}^{\mathrm{II}} 2z_1)} \qquad R_e^{\mathrm{II}} = +j\frac{(B_p^{\mathrm{II}} + A_p^{\mathrm{II}})}{\sin(k_{z_p}^{\mathrm{II}} 2z_1)},$$

$$R_h^{\mathrm{III}} = \frac{(A_k^{\mathrm{III}} + B_k^{\mathrm{III}})}{\sin(k_{y_k}^{\mathrm{III}} 2y_1)} \qquad R_e^{\mathrm{III}} = -j\frac{(A_k^{\mathrm{III}} + B_k^{\mathrm{III}})}{\sin(k_{y_k}^{\mathrm{III}} 2y_1)}. \tag{A1}$$

Matching the tangential magnetic field components leads to the following coupling expressions:

$$\sum_k Q_p^{\mathrm{I}\circ} \frac{1}{\sqrt{Y_p^{\mathrm{I}}}} \int_F t_{hp}^{\mathrm{I}\circ} H_{(x,y)k}^{\mathrm{III}}\, df = K_{pk}^{\mathrm{I,III}} R_k^{\mathrm{III}},$$

$$\sum_k Q_p^{\mathrm{II}\circ} \frac{1}{\sqrt{Y_p^{\mathrm{II}}}} \int_F t_{hp}^{\mathrm{II}\circ} H_{(x,y)k}^{\mathrm{III}}\, df = K_{pk}^{\mathrm{II,III}} R_k^{\mathrm{III}},$$

$$\sum_p Q_k^{\mathrm{III}\circ} \frac{1}{\sqrt{Y_k^{\mathrm{III}}}} \int_F t_{hk}^{\mathrm{III}\circ} H_{(x,z)p}^{\mathrm{I}}\, df = K_{kp}^{\mathrm{III,I}} R_p^{\mathrm{I}},$$

$$\sum_p Q_k^{\mathrm{III}\circ} \frac{1}{\sqrt{Y_k^{\mathrm{III}}}} \int_F t_{hk}^{\mathrm{III}\circ} H_{(x,z)p}^{\mathrm{II}}\, df = K_{kp}^{\mathrm{III,II}} R_p^{\mathrm{II}}, \tag{A2}$$

with

$$\vec{t}_h^{\,i} = \begin{pmatrix} \operatorname{grad} T_e^i \times \vec{e}_{y,z} \\ \operatorname{grad} T_h^i \end{pmatrix}. \tag{A3}$$

Y are the wave admittances, Q the normalization factors of the form:

$$Q_{pq} = \frac{1}{\sqrt{\frac{ab}{4}\left(\left(\frac{p\pi}{a}\right)^2 + \left(\frac{q\pi}{b}\right)^2\right)}} \tag{A4}$$

R are the above represented unknown amplitudes and H the corresponding magnetic field components. E.g. for the coupling between the subregions I and III (Fig. 2(a)), $H_{(x,y)}^{\mathrm{III}}$ for the four coupling cases are given by

TE to TE coupling

$$H_{\mathrm{TE-TE}}^{\mathrm{III}} = \left(\frac{1}{j} Q_k^{\mathrm{III}} \sqrt{Y_{hk}^{\mathrm{III}}} \operatorname{grad} T_{hy,xk}^{\mathrm{III}} R_{hk}^{\mathrm{III}} \cdot \cos\left(k_{yh_k}^{\mathrm{III}}(-y + y_1)\right) + \frac{1}{j\omega\mu} Q_k^{\mathrm{III}} \sqrt{Z_{hk}^{\mathrm{III}}} \cdot \Delta T_{hy,yk}^{\mathrm{III}} R_{hk}^{\mathrm{III}} \sin\left(k_{yh_k}^{\mathrm{III}}(-y + y_1)\right)\right) \tag{A5}$$

TE to TM coupling

$$H_{\mathrm{TE-TM}}^{\mathrm{III}} = Q_l^{\mathrm{III}} \sqrt{Y_{el}^{\mathrm{III}}} \operatorname{grad} T_{ey,xl}^{\mathrm{III}} \times \vec{e}_y R_{el}^{\mathrm{III}} \cdot \cos\left(k_{ye_l}^{\mathrm{III}}(-y + y_1)\right) \tag{A6}$$

TM to TE coupling

$$H_{\mathrm{TM-TE}}^{\mathrm{III}} = \left(\frac{1}{j} Q_k^{\mathrm{III}} \sqrt{Y_{hk}^{\mathrm{III}}} \operatorname{grad} T_{hy,xk}^{\mathrm{III}} R_{hk}^{\mathrm{III}} \cdot \cos\left(k_{yh_k}^{\mathrm{III}}(-y + y_1)\right) + \frac{1}{j\omega\mu} Q_k^{\mathrm{III}} \sqrt{Z_{hk}^{\mathrm{III}}} \cdot \Delta T_{hy,yk}^{\mathrm{III}} R_{hk}^{\mathrm{III}} \sin\left(k_{yh_k}^{\mathrm{III}}(-y + y_1)\right)\right) \tag{A7}$$

TM to TM coupling

$$H_{\mathrm{TM-TM}}^{\mathrm{III}} = Q_l^{\mathrm{III}} \sqrt{Y_{el}^{\mathrm{III}}} \operatorname{grad} T_{ey,xl}^{\mathrm{III}} \times \vec{e}_y R_{el}^{\mathrm{III}} \cdot \cos\left(k_{ye_l}^{\mathrm{III}}(-y + y_1)\right) \tag{A8}$$

H^{I} and H^{II} are found analogeously.

$$
\begin{array}{|c|c|c|c|}
\hline
-E + j\cot k^{\mathrm{I}}_{zh_p} & -j\dfrac{1}{\sin k^{\mathrm{II}}_{zhp}} & +j\dfrac{K^{\mathrm{I,III}}_{hh_{ph}}}{\sin k^{\mathrm{III}}_{yhk}} + j\dfrac{K^{\mathrm{I,III}}_{he_{pl}}}{\sin k^{\mathrm{III}}_{yel}} & B^{\mathrm{I}}_{hp} \\
-E + j\cot k^{\mathrm{I}}_{ze_q} & -j\dfrac{1}{\sin k^{\mathrm{II}}_{zeq}} & +j\dfrac{K^{\mathrm{I,III}}_{eh_{qk}}}{\sin k^{\mathrm{III}}_{yhk}} + j\dfrac{K^{\mathrm{I,III}}_{ee_{ql}}}{\sin k^{\mathrm{III}}_{yel}} & B^{\mathrm{I}}_{eq} \\
\hline
-j\dfrac{1}{\sin k^{\mathrm{I}}_{zhp}} & -E + j\cot k^{\mathrm{II}}_{zh_p} & -j\dfrac{K^{\mathrm{II,III}}_{hh_{pk}}}{\sin k^{\mathrm{III}}_{yhk}} - j\dfrac{K^{\mathrm{II,III}}_{he_{pl}}}{\sin k^{\mathrm{III}}_{yel}} & B^{\mathrm{II}}_{hp} \\
-j\dfrac{1}{\sin k^{\mathrm{I}}_{zeq}} & -E + j\cot k^{\mathrm{II}}_{ze_q} & -j\dfrac{K^{\mathrm{II,III}}_{eh_{qk}}}{\sin k^{\mathrm{III}}_{yhk}} - j\dfrac{K^{\mathrm{II,III}}_{ee_{ql}}}{\sin k^{\mathrm{III}}_{yel}} & B^{\mathrm{II}}_{eq} \\
\hline
+j\dfrac{K^{\mathrm{III,I}}_{hh_{kp}}}{\sin k^{\mathrm{I}}_{zhp}} + j\dfrac{K^{\mathrm{III,I}}_{he_{kq}}}{\sin k^{\mathrm{I}}_{zeq}} & -j\dfrac{K^{\mathrm{III,II}}_{hh_{kp}}}{\sin k^{\mathrm{II}}_{zhp}} - j\dfrac{K^{\mathrm{III,II}}_{he_{kq}}}{\sin k^{\mathrm{II}}_{zeq}} & -E + j\cot k^{\mathrm{III}}_{yh_k} & B^{\mathrm{III}}_{hk} \\
+j\dfrac{K^{\mathrm{III,I}}_{eh_{lp}}}{\sin k^{\mathrm{I}}_{zhp}} + j\dfrac{K^{\mathrm{III,I}}_{ee_{lq}}}{\sin k^{\mathrm{I}}_{zeq}} & -j\dfrac{K^{\mathrm{III,II}}_{eh_{lp}}}{\sin k^{\mathrm{II}}_{zhp}} - j\dfrac{K^{\mathrm{III,II}}_{ee_{lq}}}{\sin k^{\mathrm{II}}_{zeq}} & -E + j\cot k^{\mathrm{III}}_{ye_l} & B^{\mathrm{III}}_{el} \\
\hline
\end{array}
$$

$$
=
$$

$$
\begin{array}{|c|c|c|c|}
\hline
-E - j\cot k^{\mathrm{I}}_{zh_p} & +j\dfrac{1}{\sin k^{\mathrm{II}}_{zhp}} & -j\dfrac{K^{\mathrm{I,III}}_{hh_{pk}}}{\sin k^{\mathrm{III}}_{yhk}} - j\dfrac{K^{\mathrm{I,III}}_{he_{pl}}}{\sin k^{\mathrm{III}}_{yel}} & A^{\mathrm{I}}_{hp} \\
-E - j\cot k^{\mathrm{I}}_{ze_q} & +j\dfrac{1}{\sin k^{\mathrm{II}}_{zeq}} & -j\dfrac{K^{\mathrm{I,III}}_{eh_{qk}}}{\sin k^{\mathrm{III}}_{yhk}} - j\dfrac{K^{\mathrm{I,III}}_{ee_{ql}}}{\sin k^{\mathrm{III}}_{yel}} & A^{\mathrm{I}}_{eq} \\
\hline
+j\dfrac{1}{\sin k^{\mathrm{I}}_{zhp}} & -E - j\cot k^{\mathrm{II}}_{zh_p} & +j\dfrac{K^{\mathrm{II,III}}_{hh_{pk}}}{\sin k^{\mathrm{III}}_{yhk}} + j\dfrac{K^{\mathrm{II,III}}_{he_{pl}}}{\sin k^{\mathrm{III}}_{yel}} & A^{\mathrm{II}}_{hp} \\
+j\dfrac{1}{\sin k^{\mathrm{I}}_{zeq}} & -E - j\cot k^{\mathrm{II}}_{ze_q} & +j\dfrac{K^{\mathrm{II,III}}_{eh_{qk}}}{\sin k^{\mathrm{III}}_{yhk}} + j\dfrac{K^{\mathrm{II,III}}_{ee_{ql}}}{\sin k^{\mathrm{III}}_{yel}} & A^{\mathrm{II}}_{eq} \\
\hline
-j\dfrac{K^{\mathrm{III,I}}_{hh_{kp}}}{\sin k^{\mathrm{I}}_{zhp}} - j\dfrac{K^{\mathrm{III,I}}_{he_{kq}}}{\sin k^{\mathrm{I}}_{zeq}} & +j\dfrac{K^{\mathrm{III,II}}_{hh_{kp}}}{\sin k^{\mathrm{II}}_{zhp}} + j\dfrac{K^{\mathrm{III,II}}_{he_{kq}}}{\sin k^{\mathrm{II}}_{zeq}} & -E - j\cot k^{\mathrm{III}}_{yh_k} & A^{\mathrm{III}}_{hk} \\
-j\dfrac{K^{\mathrm{III,I}}_{eh_{lp}}}{\sin k^{\mathrm{I}}_{zhp}} - j\dfrac{K^{\mathrm{III,I}}_{ee_{lq}}}{\sin k^{\mathrm{I}}_{zeq}} & +j\dfrac{K^{\mathrm{III,II}}_{eh_{lp}}}{\sin k^{\mathrm{II}}_{zhp}} + j\dfrac{K^{\mathrm{III,II}}_{ee_{lq}}}{\sin k^{\mathrm{II}}_{zeq}} & -E - j\cot k^{\mathrm{III}}_{ye_l} & A^{\mathrm{III}}_{el} \\
\hline
\end{array}
\qquad \text{(A9)}
$$

Rearranging of the Equation (A9):

The equation (A9) may be abbreviated by

$$
\begin{aligned}
&+\underline{a}_{11}\underline{B}^{\mathrm{I}} - \underline{a}_{12}\underline{B}^{\mathrm{II}} + \underline{a}_{13}\underline{B}^{\mathrm{III}} \\
&\quad = +\underline{b}_{11}\underline{A}^{\mathrm{I}} + \underline{a}_{12}\underline{A}^{\mathrm{II}} - \underline{a}_{13}\underline{A}^{\mathrm{III}}, \\
&-\underline{a}_{12}\underline{B}^{\mathrm{I}} + \underline{a}_{11}\underline{B}^{\mathrm{II}} - \underline{a}_{23}\underline{B}^{\mathrm{III}} \\
&\quad = +\underline{a}_{12}\underline{A}^{\mathrm{I}} + \underline{b}_{11}\underline{A}^{\mathrm{II}} + \underline{a}_{23}\underline{A}^{\mathrm{III}}, \\
&+\underline{a}_{31}\underline{B}^{\mathrm{I}} - \underline{a}_{32}\underline{B}^{\mathrm{II}} + \underline{a}_{33}\underline{B}^{\mathrm{III}} \\
&\quad = -\underline{a}_{31}\underline{A}^{\mathrm{I}} + \underline{a}_{32}\underline{A}^{\mathrm{II}} + \underline{b}_{33}\underline{A}^{\mathrm{III}}, \qquad \text{(A10)}
\end{aligned}
$$

where a, b are the corresponding submatrices of the left and the right side of (A9), respectively.

Separation of B:

$$
\begin{aligned}
\underline{B}^{\mathrm{I}} &= \underline{M}_1\underline{B}^{\mathrm{III}} + \underline{M}_2\underline{A}^{\mathrm{I}} + \underline{M}_3\underline{A}^{\mathrm{II}} + \underline{M}_1\underline{A}^{\mathrm{III}} \\
\underline{B}^{\mathrm{II}} &= \underline{M}_4\underline{B}^{\mathrm{III}} + \underline{M}_3\underline{A}^{\mathrm{I}} + \underline{M}_2\underline{A}^{\mathrm{II}} + \underline{M}_4\underline{A}^{\mathrm{III}} \qquad \text{(A11)}
\end{aligned}
$$

with:

$$
\begin{aligned}
\underline{M}_1 &= \underline{a}_{11}^{-1}\underline{a}_{12}\underline{a}_{11}^{-1}(\underline{E} - \underline{a}_{11}^{-1}\underline{a}_{12}\underline{a}_{11}^{-1}\underline{a}_{12})^{-1}\underline{a}_{23} \\
&\quad - \underline{a}_{11}^{-1}(\underline{E} - \underline{a}_{11}^{-1}\underline{a}_{12}\underline{a}_{11}^{-1}\underline{a}_{12})^{-1}\underline{a}_{13} \\
\underline{M}_2 &= \underline{a}_{11}^{-1}\underline{a}_{12}\underline{a}_{11}^{-1}(\underline{E} - \underline{a}_{11}^{-1}\underline{a}_{12}\underline{a}_{11}^{-1}\underline{a}_{12})^{-1}\underline{a}_{12} \\
&\quad + \underline{a}_{11}^{-1}(\underline{E} - \underline{a}_{11}^{-1}\underline{a}_{12}\underline{a}_{11}^{-1}\underline{a}_{12})^{-1}\underline{b}_{11} \\
\underline{M}_3 &= \underline{a}_{11}^{-1}\underline{a}_{12}\underline{a}_{11}^{-1}(\underline{E} - \underline{a}_{11}^{-1}\underline{a}_{12}\underline{a}_{11}^{-1}\underline{a}_{12})^{-1}\underline{b}_{11} \\
&\quad + \underline{a}_{11}^{-1}(\underline{E} - \underline{a}_{11}^{-1}\underline{a}_{12}\underline{a}_{11}^{-1}\underline{a}_{12})^{-1}\underline{a}_{12}
\end{aligned}
$$

$$\underline{M}_4 = -\underline{a}_{11}^{-1}\underline{a}_{12}\underline{a}_{11}^{-1}(\underline{E} - \underline{a}_{11}^{-1}\underline{a}_{12}\underline{a}_{11}^{-1}\underline{a}_{12})^{-1}\underline{a}_{13} + \underline{a}_{11}^{-1}(\underline{E} - \underline{a}_{11}^{-1}\underline{a}_{12}\underline{a}_{11}^{-1}\underline{a}_{12})^{-1}\underline{a}_{23} \quad \text{(A12)}$$

$$\underline{B}^{III} = \underline{N}_1\underline{A}^{I} + \underline{N}_2\underline{A}^{II} + \underline{N}_3\underline{A}^{III} \quad \text{(A13)}$$

with

$$\underline{N}_1 = \underline{Y}(-\underline{a}_{31}\underline{M}_2 + \underline{a}_{32}\underline{M}_3 - \underline{a}_{31})$$
$$\underline{N}_2 = \underline{Y}(-\underline{a}_{31}\underline{M}_3 + \underline{a}_{32}\underline{M}_2 + \underline{a}_{32})$$
$$\underline{N}_3 = \underline{Y}(-\underline{a}_{31}\underline{M}_1 + \underline{a}_{32}\underline{M}_4 + \underline{b}_{33}) \quad \text{(A14)}$$

and

$$\underline{Y} = (+\underline{a}_{31}\underline{M}_1 - \underline{a}_{32}\underline{M}_4 + \underline{a}_{33})^{-1}. \quad \text{(A15)}$$

This yields the modal S-matrix:

$$\underline{B}^{I} = (\underline{M}_1\underline{N}_1 + \underline{M}_2)\underline{A}^{I} + (\underline{M}_1\underline{N}_2 + \underline{M}_3)\underline{A}^{II} + (\underline{M}_1\underline{N}_3 + \underline{M}_1)\underline{A}^{III}$$
$$\underline{B}^{II} = (\underline{M}_4\underline{N}_1 + \underline{M}_3)\underline{A}^{I} + (\underline{M}_4\underline{N}_2 + \underline{M}_2)\underline{A}^{II} + (\underline{M}_4\underline{N}_3 + \underline{M}_4)\underline{A}^{III}$$
$$\underline{B}^{III} = \underline{N}_1\underline{A}^{I} + \underline{N}_2\underline{A}^{II} + \underline{N}_3\underline{A}^{III} \quad \text{(A16)}$$

Cascaded Two-Ports a, b:

$$\underline{S}_{11}^{c} = \underline{S}_{11}^{a} + \underline{S}_{12}^{a}\underline{S}_{11}^{b}(\underline{E} - \underline{S}_{22}^{a}\underline{S}_{11}^{b})^{-1}\underline{S}_{21}^{a}$$
$$\underline{S}_{12}^{c} = \underline{S}_{12}^{a}\underline{S}_{12}^{b} + \underline{S}_{12}^{a}\underline{S}_{11}^{b}(\underline{E} - \underline{S}_{22}^{a}\underline{S}_{11}^{b})^{-1}\underline{S}_{22}^{a}\underline{S}_{12}^{b}$$
$$\underline{S}_{21}^{c} = \underline{S}_{21}^{b}(\underline{E} - \underline{S}_{22}^{a}\underline{S}_{11}^{b})^{-1}\underline{S}_{21}^{a}$$
$$\underline{S}_{22}^{c} = \underline{S}_{21}^{b}(\underline{E} - \underline{S}_{22}^{a}\underline{S}_{11}^{b})^{-1}\underline{S}_{22}^{a}\underline{S}_{12}^{b} + \underline{S}_{22}^{b} \quad \text{(A17)}$$

Cascaded Two- and Three-Port:

$$\underline{S}_{11}^{c} = \underline{S}_{11}^{a} + \underline{S}_{12}^{a}\underline{T}_2\underline{S}_{21}^{a} \quad \underline{S}_{12}^{c} = \underline{S}_{12}^{a}\underline{S}_{12}^{b} + \underline{S}_{12}^{a}\underline{T}_2\underline{T}_4$$
$$\underline{S}_{13}^{c} = \underline{S}_{13}^{a} + \underline{S}_{12}^{a}\underline{T}_2\underline{S}_{23}^{a} \quad \underline{S}_{21}^{c} = \underline{T}_3\underline{S}_{21}^{a}$$
$$\underline{S}_{22}^{c} = \underline{S}_{22}^{b} + \underline{T}_3\underline{T}_4 \quad \underline{S}_{23}^{c} = \underline{T}_3\underline{S}_{23}^{a}$$
$$\underline{S}_{31}^{c} = \underline{S}_{31}^{a} + \underline{S}_{32}^{a}\underline{T}_2\underline{S}_{21}^{a} \quad \underline{S}_{32}^{c} = \underline{S}_{32}^{a}\underline{S}_{12}^{b} + \underline{S}_{32}^{a}\underline{T}_2\underline{T}_4$$
$$\underline{S}_{33}^{c} = \underline{S}_{33}^{a} + \underline{S}_{32}^{a}\underline{T}_2\underline{S}_{23}^{a} \quad \text{(A18)}$$

with

$$\underline{T}_1 = \underline{E} - \underline{S}_{22}^{a}\underline{S}_{11}^{b} \quad \underline{T}_2 = \underline{S}_{11}^{b}T_1^{-1}$$
$$\underline{T}_3 = \underline{S}_{21}^{b}T_1^{-1} \quad \underline{T}_4 = \underline{S}_{22}^{a}\underline{S}_{12}^{b} \quad \text{(A19)}$$

Cascaded Three-Ports a, b:

$$\underline{S}_{11}^{c} = \underline{S}_{11}^{a} + \underline{T}_8\underline{S}_{31}^{a} \quad \underline{S}_{21}^{c} = \underline{S}_{21}^{a} + \underline{T}_9\underline{S}_{31}^{a}$$
$$\underline{S}_{12}^{c} = \underline{S}_{12}^{a} + \underline{T}_8\underline{S}_{32}^{a} \quad \underline{S}_{22}^{c} = \underline{S}_{22}^{a} + \underline{T}_9\underline{S}_{32}^{a}$$
$$\underline{S}_{13}^{c} = \underline{S}_{13}^{a}\underline{T}_6 \quad \underline{S}_{23}^{c} = \underline{S}_{23}^{a}\underline{T}_6$$
$$\underline{S}_{14}^{c} = \underline{S}_{13}^{a}\underline{T}_7 \quad \underline{S}_{24}^{c} = \underline{S}_{23}^{a}\underline{T}_7$$
$$\underline{S}_{31}^{c} = \underline{S}_{13}^{b}\underline{T}_5\underline{S}_{31}^{a} \quad \underline{S}_{41}^{c} = \underline{S}_{23}^{b}\underline{T}_5\underline{S}_{31}^{a}$$
$$\underline{S}_{32}^{c} = \underline{S}_{13}^{b}\underline{T}_5\underline{S}_{32}^{a} \quad \underline{S}_{42}^{c} = \underline{S}_{23}^{b}\underline{T}_5\underline{S}_{32}^{a}$$
$$\underline{S}_{33}^{c} = \underline{S}_{11}^{b} + \underline{T}_{10}\underline{S}_{31}^{b} \quad \underline{S}_{43}^{c} = \underline{S}_{21}^{b} + \underline{T}_{11}\underline{S}_{31}^{b}$$
$$\underline{S}_{34}^{c} = \underline{S}_{12}^{b} + \underline{T}_{10}\underline{S}_{32}^{b} \quad \underline{S}_{44}^{c} = \underline{S}_{22}^{b} + \underline{T}_{11}\underline{S}_{32}^{b} \quad \text{(A20)}$$

with

$$T_5 = (\underline{E} - \underline{S}_{33}^{a}\underline{S}_{33}^{b})^{-1} \quad \underline{T}_6 = \underline{S}_{31}^{b} + \underline{S}_{33}^{b}\underline{T}_5\underline{S}_{33}^{a}\underline{S}_{31}^{b}$$
$$\underline{T}_7 = \underline{S}_{32}^{b} + \underline{S}_{33}^{b}\underline{T}_5\underline{S}_{33}^{a}\underline{S}_{32}^{b} \quad \underline{T}_8 = \underline{S}_{13}^{a}\underline{S}_{33}^{b}\underline{T}_5$$
$$\underline{T}_9 = \underline{S}_{23}^{a}\underline{S}_{33}^{b}\underline{T}_5 \quad \underline{T}_{10} = \underline{S}_{13}^{b}\underline{T}_5\underline{S}_{33}^{a}$$
$$\underline{T}_{11} = \underline{S}_{23}^{b}\underline{T}_5\underline{S}_{33}^{a} \quad \text{(A21)}$$

References

[1] N. Marcuvitz, *Waveguide Handbook*. New York: McGraw-Hill, 1951.

[2] L. Matthaei, L. Young, and E. M. T. Jones, *Microwave Filters, Impedance Matching Networks, and Coupling Structures*. New York: McGraw-Hill, 1964.

[3] E. D. Sharp, "An exact calculation for a T-junction of rectangular waveguides having arbitrary cross sections," *IEEE Trans. Microwave Theory Tech.*, vol. MTT-15, pp. 109–116, Feb. 1967.

[4] J. D. Rhodes and R. Levy, "Design of general manifold multiplexers," *IEEE Trans. Microwave Theory Tech.*, vol. MTT-27, pp. 111–123, Feb. 1979.

[5] R. Levy, "Improved single and multiaperture waveguide coupling theory, including explanation of mutual interactions," *IEEE Trans. Microwave Theory Tech.*, vol. MTT-28, pp. 331–338, Apr. 1980.

[6] V. M. Pandharipande and B. N. Das, "Coupling of waveguides through large apertures," *IEEE Trans. Microwave Theory Tech.*, vol. MTT-26, pp. 209–212, Mar. 1978.

[7] A. J. Sangster, "Slot coupling between uniform rectangular waveguides," *IEEE Trans. Microwave Theory Tech.*, vol. MTT-27, pp. 705–707, June 1979.

[8] B. N. Das, N. V. S. Narashima Sarma, and A. Chakraborty, "A rigorous variational formulation of an H plane slot-coupled Tee junction," *IEEE Trans. Microwave Theory Tech.*, vol. 38, pp. 93–95, Jan. 1990.

[9] H. Patzelt, and F. Arndt, "Double-plane steps in rectangular waveguides and their application for transformers, irises, and filters," *IEEE Trans. Microwave Theory Tech.*, vol. MTT-30, pp. 771–776, May 1982.

[10] J. Dittloff and F. Arndt, "Rigorous field theory design of millimeter-wave E-plane integrated circuit multiplexers," *IEEE Trans. Microwave Theory Tech.*, vol. 37, pp. 340–350, Feb. 1989.

[11] J. Bornemann, "A new class of E-plane integrated millimeter-wave filters," in *1989 IEEE MTT-S Int. Microwave Symp. Dig.*, pp. 599–602.

[12] F. Arndt, I. Ahrens, U. Papziner, U. Wiechmann, and R. Wilkeit, "Optimized E-plane T-junction series power dividers," *IEEE Trans. Microwave Theory Tech.*, vol. MTT-35, pp. 1052–1059, Nov. 1987.

[13] E. Collin, *Field Theory of Guided Waves*. New York: McGraw Hill, 1960.

[14] H. Schmiedel and F. Arndt, "Numerical synthesis of simple waveguide mode sensors," in *Proc. European Microwave Conf*, Nuremberg, Sept. 1983, pp. 733–738.

[15] W. Hanyang and W. Mei, "Moment method analysis of a feeding system in slotted waveguide antenna," in *Proc. Inst. Elec. Eng.*, pt. H, no. 5, pp. 313–318, Oct. 1988.

[16] A. A. Oliner, "The impedance properties of narrow radiating slots in the broad face of rectangular waveguide: Part I—Theory," *IRE Trans. Antennas Propagat.*, vol. 19, pp. 24–38, Jan. 1957.

[17] B. N. Das and P. V. D. Somasekhar Rao, "Analysis of cascaded sections of T junctions between rectangular and circular waveguides," *IEEE Trans. Microwave Theory Tech.*, vol. 39, pp. 92–97, Jan. 1991.
[18] S. J. Fiedziuszko, "Dual-mode dielectric resonator loaded cavity filters," *IEEE Trans. Microwave Theory Tech.*, vol. MTT-30, pp. 1311–1316, Sept. 1982.
[19] F. Arndt, T. Duschak, U. Papziner, and P. Rolappe, "Asymmetric iris coupled cavity filters with stopband poles," in *IEEE MTT-S Int. Microwave Symp. Dig.*, pp. 215–218, 1990.

Thomas Sieverding, was born in Lohne, Oldenburg, Germany, on November 28, 1959. He received the Dipl.Ing. and Dr.-Ing. degrees, both in electrical engineering, from the University of Bremen, Germany, in 1984 and 1990, respectively.

From 1985 and 1987 he worked on software engineering at BICC Vero Electronics, Bremen. Since 1987 he has been with the Microwave Department of the University of Bremen and with OTCE-Consulting. He has been an Assistant Professor at the University of Bremen since early 1991. His research deals mainly with the computer aided design of rectangular waveguide components (analysis and synthesis of couplers, junctions, and filters).

Fritz Arndt (SM'83) received the Dipl.Ing., Dr.Ing., and Habilitation degrees from the Technical University of Darmstadt, Germany, in 1963, 1968, and 1972, respectively.

From 1963 to 1973, he worked on directional couplers and microstrip techniques at the Technical University of Darmstadt. Since 1972, he has been a Professor and Head of the Microwave Department of the University of Bremen, Germany. His research activities are in the area of the solution of field problems of waveguide, finline, and optical waveguide structures, of antenna design, and of scattering structures.

Dr. Arndt is member of the VDE and NTG (Germany). He received the NTG award in 1970, the A. F. Bulgin Award (together with three coauthors) from the Institution of Radio and Electronic Engineers in 1983, and the best paper award of the antenna conference JINA 1986 (France).